Methods for comparing uncertainty quantifications for material property predictions

Kevin Tran,[†,¶] Willie Neiswanger,[‡,¶] Junwoong Yoon,[†] Eric Xing,[‡] and Zachary W. Ulissi[*,†]

†*Chemical Engineering Department, Carnegie Mellon University, Pittsburgh, PA 15217*

‡*Machine Learning Department, Carnegie Mellon University, Pittsburgh, PA 15217*

¶*These authors contributed equally to this work*

E-mail: zulissi@andrew.cmu.edu

Abstract

Data science and informatics tools have been proliferating recently within the computational materials science and catalysis fields. This proliferation has spurred the creation of various frameworks for automated materials screening, discovery, and design. Underpinning these frameworks are surrogate models with uncertainty estimates on their predictions. These uncertainty estimates are instrumental for determining which materials to screen next, but the computational catalysis field does not yet have a standard procedure for judging the quality of such uncertainty estimates. Here we present a suite of figures and performance metrics derived from the machine learning community that can be used to judge the quality of such uncertainty estimates. This suite probes the accuracy, calibration, and sharpness of a model quantitatively. We then show a case study where we judge various methods for predicting density-functional-theory-calculated adsorption energies. Of the methods studied here, we find that the best performer is a model where a convolutional neural network is used

1

to supply features to a Gaussian process regressor, which then makes predictions of adsorption energies along with corresponding uncertainty estimates.

Introduction

The fields of catalysis and materials science are burgeoning with methods to screen, design, and understand materials.[1–4] This research has spurred the creation of Machine Learning (ML) models to predict various material properties. Unfortunately, the design spaces for these models are sometimes too large and intractable to sample completely. These under-sampling issues can limit the training data and therefore the predictive power of the models. It would be helpful to have an uncertainty quantification (UQ) for a model so that we know when to trust the predictions and when not to. More specifically: UQ would enable various online, active frameworks for materials discovery and design (e.g., active learning,[5] online active learning,[6] Bayesian optimization,[7] active search,[8] or goal oriented design of experiments[9]).

Such active frameworks have already been used successfully in the field of catalysis and materials informatics. For example: Peterson[10] has used a neural network to perform online active learning of nudged elastic band (NEB) calculations, reducing the number of force calls by an order of magnitude. Torres et al.[11] have also used online active learning to accelerate NEB calculations, but they used a Gaussian Process (GP) model instead of a neural network. Jinnouchi et al.[12] have used online active learning to accelerate molecular dynamics simulations. These methods are all underpinned by models with UQ, which have garnered increasing attention.[13,14]

The goal of UQ is to quantify accurately the likelihood of outcomes associated with a predicted quantity. For example, given an input for which we wish to make a prediction, a predictive UQ method might return a confidence interval that aims to capture the true outcome a specified percentage of the time or might return a probability distribution over

possible outcomes. Performance metrics for predictive UQ methods aim to assess how well a given quantification of the probabilities of potential true outcomes adheres to a set of observations of these outcomes. Some of the performance metrics for predictive UQ are agnostic to prediction performance—they provide an assessment of the uncertainty independent of the predictive accuracy (i.e. a method can predict badly, but could still accurately quantify its own uncertainty).

We have seen few[15] comparisons of different methods for UQ within the field of catalysis and materials informatics. Here we examine a protocol[16] for comparing the performance of different modeling and UQ methods (Figure 1). We then illustrate the protocol on a case study where we compare various models' abilities to predict Density Functional Theory (DFT) calculated adsorption energies. We also offer anecdotal insights from our case study. We acknowledge that such insights may not be transferable to other applications, but we find value in sharing them so that others can build their own intuition.

Methods

Dataset information

All regressions in this paper were performed using a dataset of 47,279 DFT calculated adsorption energies created with the Generalized Adsorption Simulator for Python (GASpy).[17,18] Within this dataset, there were 52 different elements within the 1,952 bulk structures used as bases for the adsorption surfaces. The 61 bulk structures that contained one element encompassed 5,844 of the adsorption calculations; the 1,057 bulk structures that contained two elements encompassed 31,651 of the calculations; the 774 bulk structures that contained three elements encompassed 9,139 of the calculations; and the 60 bulk structures that contained four or five elements encompassed 645 of the calculations. The dataset also comprised 9,102 symmetrically distinct surfaces and 29,843 distinct coordination environments (as defined by the surface and the adsorbate neighbors). Lastly, the dataset was comprised of
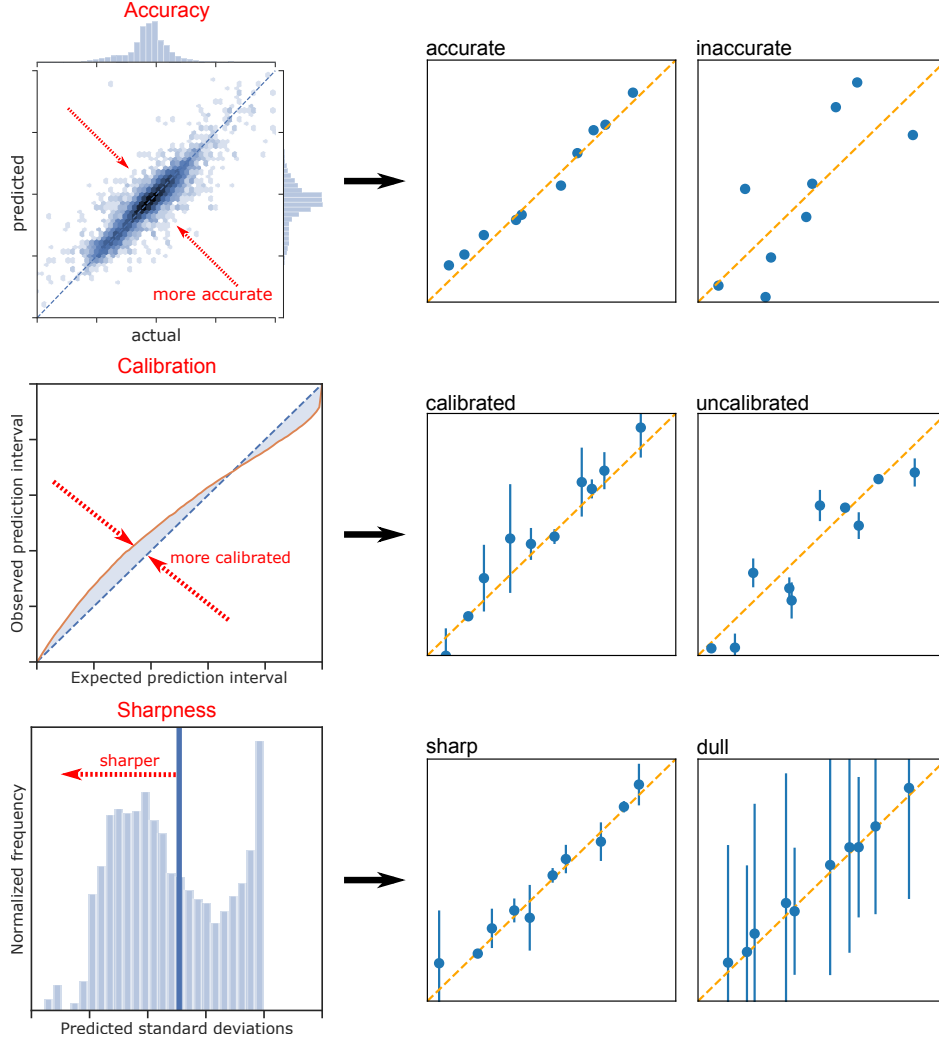
Figure 1: Overview of proposed procedure for judging the quality of models with uncertainty estimates. First and foremost, the models should be accurate. Second, the models should be "calibrated", which means that their uncertainty estimates should be comparable with their residuals. Third, the models should be "sharp", which means that their uncertainty estimates should be narrow. This study demonstrates how to visualize and quantify these characteristics so that different methods of UQ can be compared objectively.

21,269 H adsorption energies; 18,437 CO adsorption energies; 3,464 OH adsorption energies; 2,515 O adsorption energies; and 1,594 N adsorption energies.

GASpy performed all DFT calculations using the Vienna Ab-initio Simulation Package (VASP)[19–22] version 5.4 implemented in the Atomic Simulation Environment (ASE).[23] The revised Perdew-Burke-Ernzerhof (rPBE) functionals[24] were used along with VASP's pseudopotentials, and no spin magnetism or dispersion corrections were used. Bulk relaxations were performed with a $10 \times 10 \times 10$ k-point grid and a 500 electron volts (eV) cutoff, and only isotropic relaxation were allowed during this bulk relaxation. Slab relaxations were performed with k-point grids of $4 \times 4 \times 1$ and a 350 eV cutoff. Slabs were replicated in the X/Y directions so that each cell was at least 4.5 Å wide, which reduces adsorbate self-interaction. Slabs were also replicated in the Z direction until they were at least 7 Å thick, and at least 20 Å of vacuum was included in between slabs. The bottom layers of each slab were fixed and defined as those atoms more than 3 Å from the top of the surface in the scaled Z direction.

To split the data into train/validate/test sets, we enumerated all adsorption energies on monometallic slabs and added them to the training set manually. We did this because some of the regression methods in this paper use a featurization that contains our monometallic adsorption energy data,[17] and so having the monometallic adsorption energies pre-allocated in the training set prevented any information leakage between the training set and validation/test sets. After this allocation, we performed a 64/14/20 train/validate/test split that was stratified[25] by adsorbate. We then used the validation set's results to tune various hyperparameters manually. After tuning, we calculated the test set results and present them in this paper exclusively. Note that the test results were obtained using models that were trained only using the training set, not the validation set. This is acceptable because we only seek to compare methods here, not to optimize them.

Regression methods

We explore various methods that aim to quantify the uncertainty for regression procedures where the predicted quantity is a continuous variable. To standardize the assessment of performance, we ensure that each UQ method returns predictive uncertainty results in a consistent format: a distribution over possible outcomes of the predicted quantity for any specified input point. This result format allows us to compute all the predictive uncertainty performance metrics which we introduce in subsequent sections. Figure 2 illustrates all of the methods we investigate in this study, and we describe each method in detail below.

NN: To establish a baseline for predictive accuracy, we re-trained a previously reported crystal graph convolutional Neural Network (NN)[26,27] on this study's training set. This NN model projects a three-dimensional atomic structure into a graph, which is then fed into convolutional layers to extract local atomic information for predicting global target properties. In this case, we predict DFT-calculated adsorption energies, ΔE. The graph consists of nodes representing atoms and edges representing distances between atoms. The NN updates the node features using the local information extracted in the convolutional layers, then hidden layers in the NN maps the node features to the adsorption energies. Reference Back et al.[27] for additional details.

NN Ensemble: We created an ensemble of NNs by 5-fold subsampling the training data and then training individual NN models on the 5 folds. Each individual NN model's architecture is identical to the base NN architecture outlined previously. The only differences are their training sets and their individually randomized initial weights. For the final prediction of the ensemble we computed the mean of the set of models' predictions, and for the ensemble's estimate of uncertainty we computed the standard deviation of the set of predictions.

BNN: The aim of Bayesian Neural Network (BNN) is to determine the posterior distribution of model parameters rather than a single optimal value of the parameters. In practice, inferring true posterior distributions is very difficult and even infeasible in most cases. Thus,
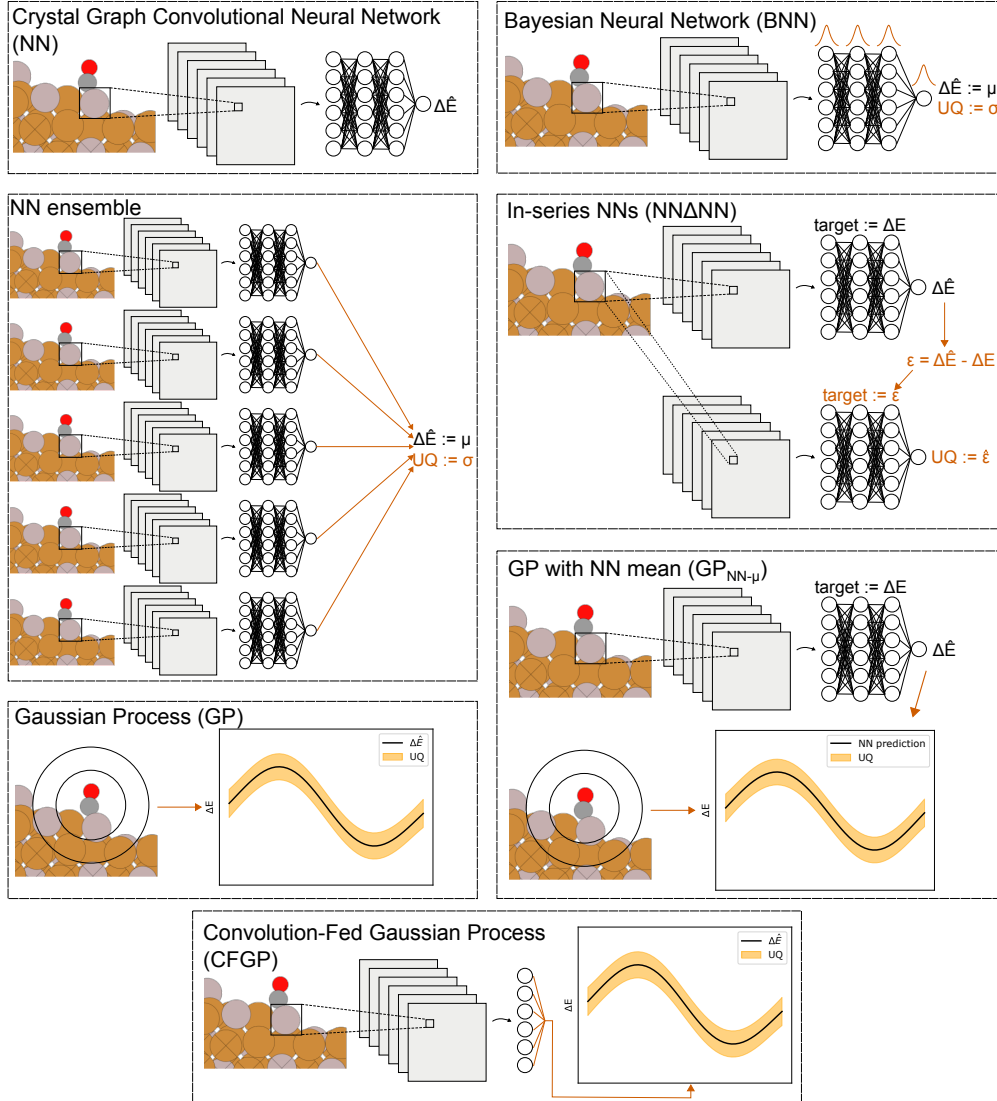
Figure 2: Overview of the various UQ methods we investigated in this study. ΔE represents DFT-calculated adsorption energies; $\Delta \hat{E}$ represents ML-predicted adsorption energies; UQ represents ML-predicted uncertainty quantifications; μ represents the mean of a sample of points; σ represents the standard deviation of a sample of points; ϵ represents the residuals between DFT and ML; and $\hat{\epsilon}$ represents the residuals between ML-predicted ϵ and the actual ϵ.

we approximate the model posterior to be as close as possible to the true posterior. The same NN architecture was used, but we converted the NN into BNN by assigning posterior distributions to all model parameters in the hidden layers in the NN model. The BNN then approximated the true posterior distributions using variational inference so that it could use the approximated posterior to predict the adsorption energies. We sampled the model parameters 20 times from the approximated posterior distributions, and used the mean of these predictions as the final prediction and the standard deviation of these predictions as the estimation of uncertainty. We implemented the BNN and performed variational inference using Pyro.[28]

NNΔNN: Suppose we have trained a NN. We may aim to empirically fit an additional mapping that predicts the error of the first NN. Here we show in-series NNs (NNΔNN), which trains a secondary NN to predict the residuals of the initial NN. When training the first NN, we hold out 10% of the training data. Afterwards, we use the residuals of the initial NN on the held-out portion as training data for the second NN. After the secondary training, this second NN can predict residuals for the first NN on some new set of input data. The predictions of the second NN can then be used as uncertainty estimates. Note that both the NNs included within the NNΔNN were constructed using the same convolutional architecture outlined previously.

GP: GPs are one of the most common regression methods for producing UQs, and so we use them here as a baseline. We fit a standard GP using the same exact features that we used in previous work.[17] These features are defined by the elements coordinated with the adsorbate and by the elements of its next-nearest neighbors. Specifically: We use the atomic numbers of these elements, their Pauling electronegativity, a count of the number of atoms of each element near the adsorbate, and the median adsorption energy between the adsorbate and the elements. To ensure that these features interacted well with the GP's kernel, we normalized each of the features to have a mean of zero and standard deviation of one. Reference Tran and Ulissi[17] for additional details. To define the GP, we assumed

a constant mean and used a Matern covariance kernel. We trained the length scale of the Matern kernel using the Maximum Likelihood Estimation (MLE) method. All GP training and predictions were done with GPU acceleration as implemented in GPyTorch.[29]

$\mathbf{GP}_{NN-\mu}$: GPs are Bayesian models in which a prior distribution is first specified and then updated given observations to yield a posterior distribution. The mean of this posterior distribution is used for regression, and the covariance matrix is used for UQ. Typically, in lieu of any additional prior knowledge, practitioners will take the prior distribution to have zero-mean. However, we could instead supply an alternative curve for the prior mean, and then perform the usual Bayesian updates to compute the posterior of this GP given observations. Here, for the GP prior mean, we supply the prediction given by a single pre-trained NN. We call this method GP with NN mean ($GP_{NN-\mu}$). For the input features of this GP, we used the same exact features we used for the plain GP—i.e., the vector of atomic numbers, electronegativity, etc. For the covariance kernel of this GP, we used a Matern kernel where we fit the kernel hyperparameters using MLE. All GP training and predictions were done with GPU acceleration as implemented in GPyTorch.[29]

CFGP: A limitation of using this formulation of a GP with NN-predicted mean is that it requires the use of hand-crafted features for the GP. This requirement reduces the transferability of the method to other applications where such features may not be readily available. To address this, we formulated a different method where we first train a NN (as described previously) to predict adsorption energies and then fix the network's weights. Then we use the 46 pooled outputs of the convolutional layers of the network as features in a new GP. The GP would then be trained to use these features to produce both mean and uncertainty predictions on the adsorption energies. We call this a Convolution-Fed Gaussian Process (CFGP). Note that we normalized the 46 convolution outputs of the NN so that each output would have a mean of zero and a standard deviation of one across the training set. To define the GP, we assumed a constant mean and used a Matern covariance kernel. We trained the length scale of the Matern kernel using the MLE method. All GP training and predictions

were done with GPU acceleration as implemented in GPyTorch.[29]

Performance metrics

We used five different metrics to quantify the accuracy of the various models: Median Absolute Error (MDAE), Root Mean Squared Error (RMSE), Mean Absolute Error (MAE), Mean Absolute Relative Percent Difference (MARPD), and R^2 correlation coefficient (R^2). We used MDAE because is insensitive to outliers and is therefore a good measure of accuracy for the majority of the data. We used RMSE because it is sensitive to outliers and is therefore a good measure of worst-case accuracy. We used MAE because it lies between MDAE and RMSE in terms of sensitivity to outliers. We used MARPD and R^2 because they provide normalized measures of accuracy that may be more interpretable for those unfamiliar with adsorption energy measurements in eV. MARPD values were calculated with Equation 1 where n is the index of a data point, N is the total number of data points, x_n is the true value of the data point, and $\hat{x}_n$ is the model's estimate of x_n. In this case, x_n is a DFT-calculated adsorption energy and $\hat{x}_n$ is the surrogate-model-calculated adsorption energy. The ensemble of these metrics provide a more robust view of accuracy than any one metric can provide alone.

$$MARPD = \frac{1}{N} \sum_{n=1}^{N} \left| 100 \cdot \frac{\hat{x}_n - x_n}{|\hat{x}_n| + |x_n|} \right| \tag{1}$$

To assess the calibration (or "honesty") of these models' UQs, we created calibration curves. A calibration curve "displays the true frequency of points in each interval relative to the predicted fraction of points in that interval", as outlined by Kuleshov et al.[16]. In other words: We used the standard deviation predictions to create Gaussian random variables for each test point and then tested how well the residuals followed their respective Gaussian random variables. Thus "well-calibrated" models had residuals that created Gaussian distributions whose standard deviations were close to the model's predicted standard devi-

ations. We discuss calibration curves in more detail in the Results section alongside specific examples. We also calculated the calibration errors[16] of our models, which is a quantitative measure of calibration.

As Kuleshov et al.[16] also pointed out, well-calibrated models are necessary but not sufficient for useful UQs. For example: A well-calibrated model could still have large uncertainty estimates, which are inherently less useful than well-calibrated and small uncertainty estimates. This idea of having small uncertainty estimates is called "sharpness", and Kuleshov et al.[16] define it with Equation 2

$$sha = \frac{1}{N} \sum_{n=1}^{N} var(F_n) \tag{2}$$

where $var(F_n)$ is the variance of the random variable whose cumulative distribution function is F at point n. This is akin to the average variance of the uncertainty estimates on the test set. Here we propose and use a new formulation (Equation 3) where we add a square root operation. This operation gives the sharpness the same units as the predictions, which provides us with a more intuitive reference. In other words: Sharpness is akin to the average of the ML-predicted standard deviations.

$$sha = \sqrt{\frac{1}{N} \sum_{n=1}^{N} var(F_n)} \tag{3}$$

We also assessed the performance of each predictive uncertainty method by comparing their negative log-likelihood (NLL) values the test set. For each test point, we established a Gaussian probability distribution using the mean and uncertainty predictions of each UQ model. Then we calculated the conditional probability of observing the true value of the test point given the probability distribution created from the UQ; this is the likelihood of one test point. We then calculated the product of all the likelihoods of all test points, which yielded the total test likelihood. It follows that better UQ methods yield higher total likelihood values. Equivalently, we could calculate the natural logarithms of each likelihood,

sum them, and then take the negative of this value; this is NLL. Equation 4 shows how we calculated NLL, where y_i is the true value of a test point, $\hat{y}_i$ is a model's predicted mean value at that test point, $\hat{\sigma}_i^2$ is the model's predicted variance at that test point, n is the set of all test points, and $N(x, y)$ is a normal distribution with mean x and variance y.

$$NLL = -\sum_{i=1}^{n} \ln P(y_i | N(\hat{y}_i, \hat{\sigma}_i^2)) \tag{4}$$

Note how the NLL value depends on the size and location of the test set. This means that the absolute value of NLL changes from application to application, and so a "good" NLL value must be contextualized within a particular test set. Within a test set, a lower NLL value indicates a better fit. We also note that we assumed Gaussian distributions for our UQ methods' predictions. This assumption does not necessarily need to be applied, meaning that the normal distribution in Equation 4 may be replaced with any other appropriate distribution.

We use NLL because it provides an overall assessment that is influenced by both the predictive accuracy of a method as well as the quality of its UQ. Previous work[30,31] has shown the NLL to be a strictly proper scoring rule, which intuitively means that it provides a fair quantitative assessment (or score) for the performance of the UQ method, and that it can be decomposed into terms that relate to both calibration and sharpness. NLL is also a popular performance metric that has been used to quantify uncertainty in a variety of prior work[32] and provides an additional single score for UQ methods.

Results

Illustrative examples

Let us first discuss the results of our NN ensemble for illustrative purposes. Figure 3 contains a parity plot, calibration curve, and predicted-uncertainty distribution of our NN ensemble

model. The parity plot shows the accuracy of the model; the calibration curve shows the
honesty of the model's uncertainty predictions; and the uncertainty distribution shows the
sharpness of the model's uncertainty predictions. Accurate models have parity plots whose
points tend to fall near the diagonal parity line. Calibrated models have calibration curves
that approach the ideal diagonal line. Sharp models have uncertainty distributions that tend
towards zero. Note that sharpness should not be won at the cost of calibration.

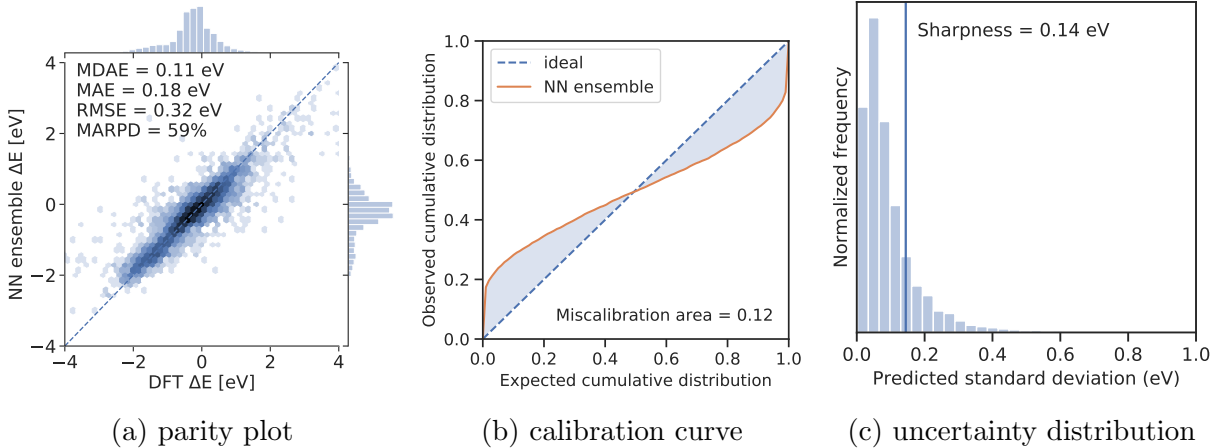(a) parity plot   (b) calibration curve   (c) uncertainty distribution

Figure 3: Results of the NN ensemble. Each figure here was created with the test set of
8,289 points.

The calibration curve was created by first establishing Gaussian random variables for
each test point where the means were the model's predictions and the variances were the
model's predicted variances. The test residuals could then be compared against their respec-
tive random variables. For simplification purposes, we divided each of the test residuals by
their corresponding standard deviations so that we could test all residuals against the same
unit Gaussian distribution. Thus if the normalized test residuals followed a unit Gaussian
distribution, then the model's uncertainty predictions could be considered well-calibrated.
We tested this by calculating the theoretical cumulative distribution of points within the
intervals $(-\infty, x] \ \forall \ x \in (-\infty, \infty)$ and then compared it against the observed cumulative
distributions. A plot of the observed cumulative distributions against the theoretical cu-
mulative distributions is called a calibration curve. A perfectly calibrated model would

have normalized residuals that are Gaussian, which would yield a diagonal calibration line. Therefore, models' calibration could be qualified by the closeness of their calibration curves to this ideal, diagonal curve. We quantified this closeness by calculating the area between the calibration curve and the ideal diagonal. We call this the miscalibration area, and smaller values indicate better calibration. We also calculated the calibration error,[16] which is the mean square difference between the expected cumulative distributions and observed cumulative distributions.

The shape of a calibration curve could also yield other insights. If a model's UQs were too low/confident, then the normalized residuals would be too large and they would fall outside their distributions too frequently. This would result in a lower observed cumulative distributions compared to the expected cumulative distributions, which would correspond to a calibration curve that falls below the ideal diagonal. Therefore, overconfident models yield calibration curves that fall under the ideal diagonal, and underconfident models yield calibration curves that fall over the ideal diagonal. Figure 4 illustrates this point by plotting calibration curves of various models alongside their parity plots that contain error bars corresponding to ±2 standard deviations. Note that when we say a calibration curve "falls under the diagonal", we allude to curves whose right-hand-side fall under the diagonal.

Summary results

Figure 5 contains parity plots for all UQ methods studied here; Figure 6 contains all calibration curves; and Figure 7 contains all distribution plots of the ML-predicted UQs. These figures illustrate the accuracy, calibration, and sharpness of the different UQ methods, respectively. Table 1 lists their performance metrics.

Regarding accuracy: All methods' MDAE results are virtually identical, and their MAE results are within 10% of each other. This suggests that all methods have comparable predictive accuracies for inliers. The plain GP has a higher RMSE value than the rest of the methods, indicating that it has the worst predictive accuracy for outliers.
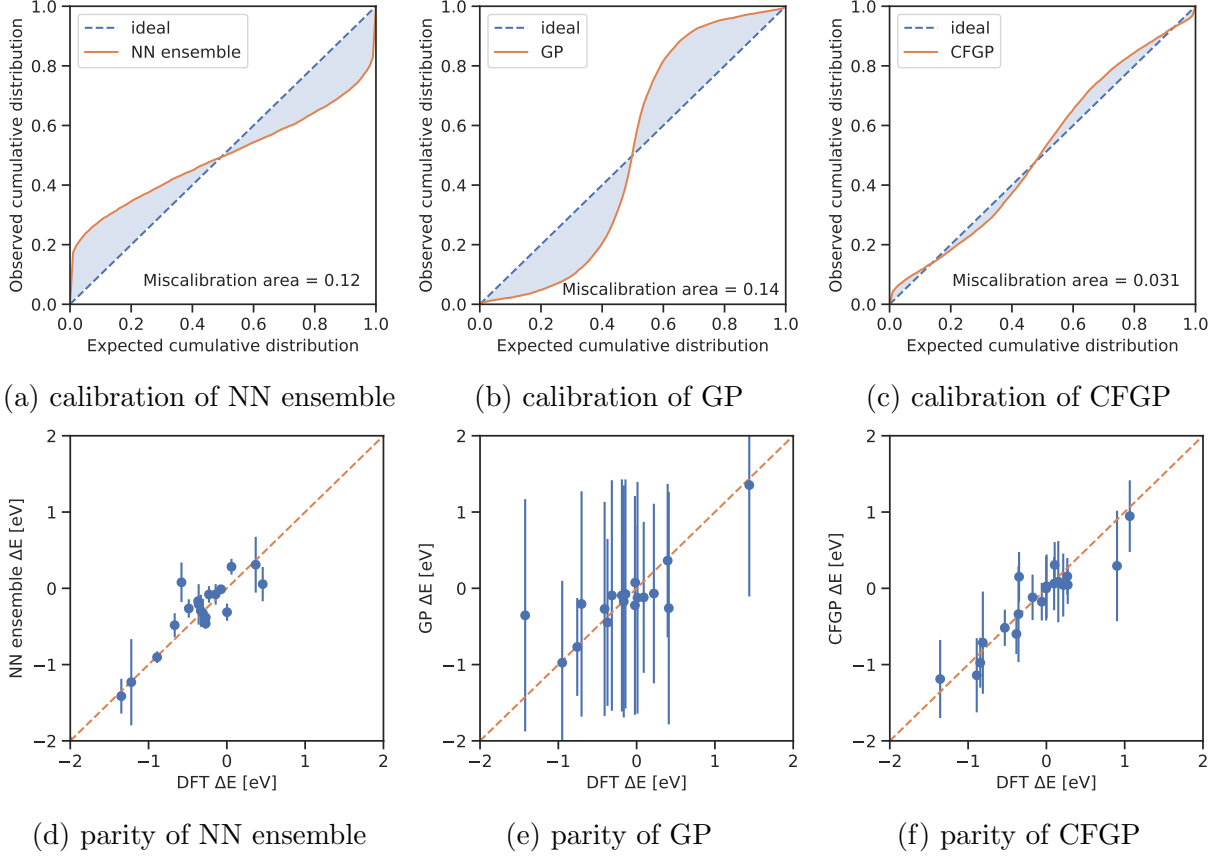
14

Figure 4: Calibration curves and parity plots of an overconfident NN ensemble, an underconfident GP, and better-calibrated CFGP. The vertical uncertainty bands in the parity plots indicate ±2 standard deviations in the uncertainty predictions of each model. For clarity, we sampled only 20 points of the 8,289 test points to put in the parity plots. It follows that relatively overconfident models would have more points with uncertainty bands that do not cross the diagonal parity line; relatively underconfident models would have more points that cross the diagonal parity line; and a well-calibrated model would have *ca.* 19 out of 20 points cross the parity line.

(a) NN ensemble   (b) BNN   (c) NNΔNN

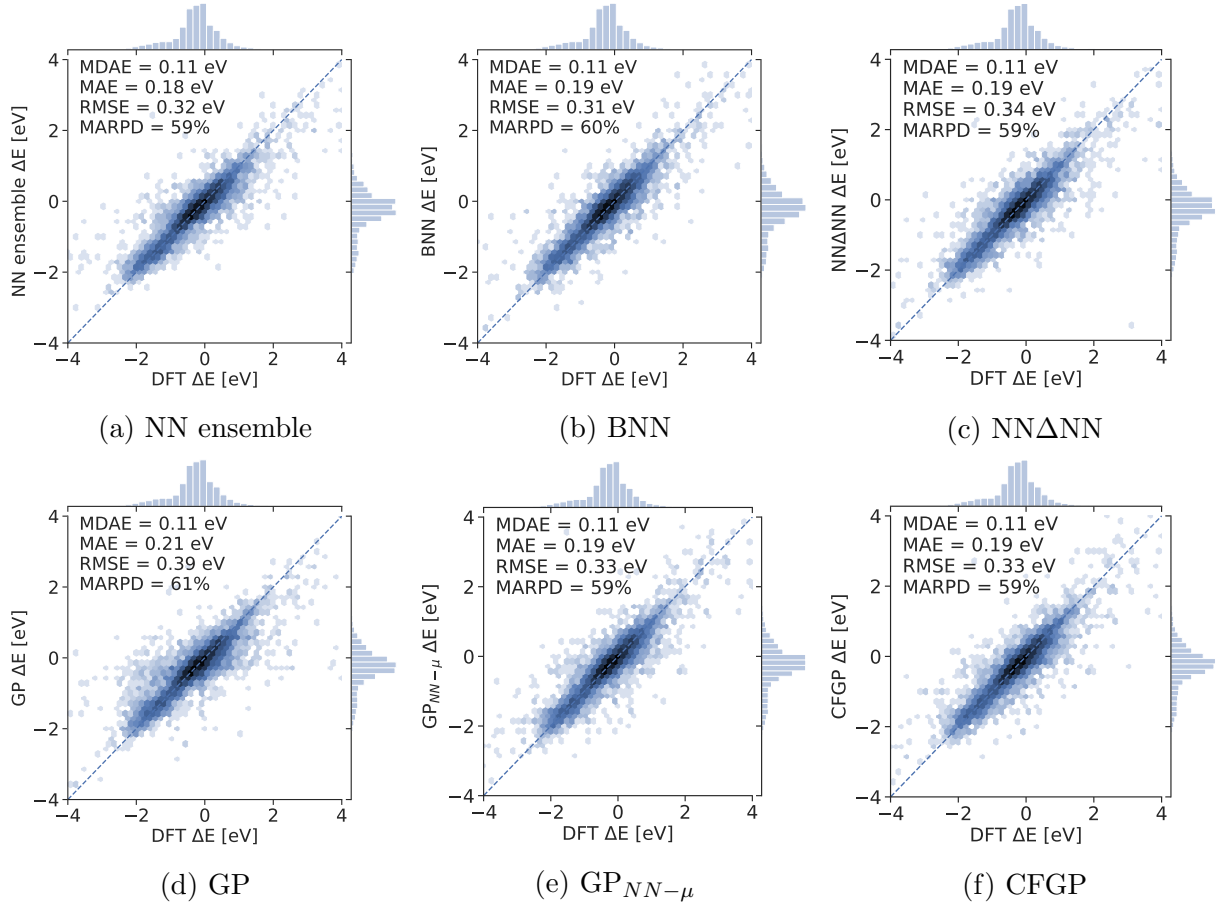(d) GP   (e) GP$_{NN-\mu}$ (f) CFGP

Figure 5: Parity plots for all UQ methods used in this study. Shading plots were used in lieu of scatter plots because the large number of test points (8,289) obfuscated patterns. Darker shading indicates a higher density of points. Logarithmically scaled shading was used to accentuate outliers. The dashed, diagonal lines indicate parity.
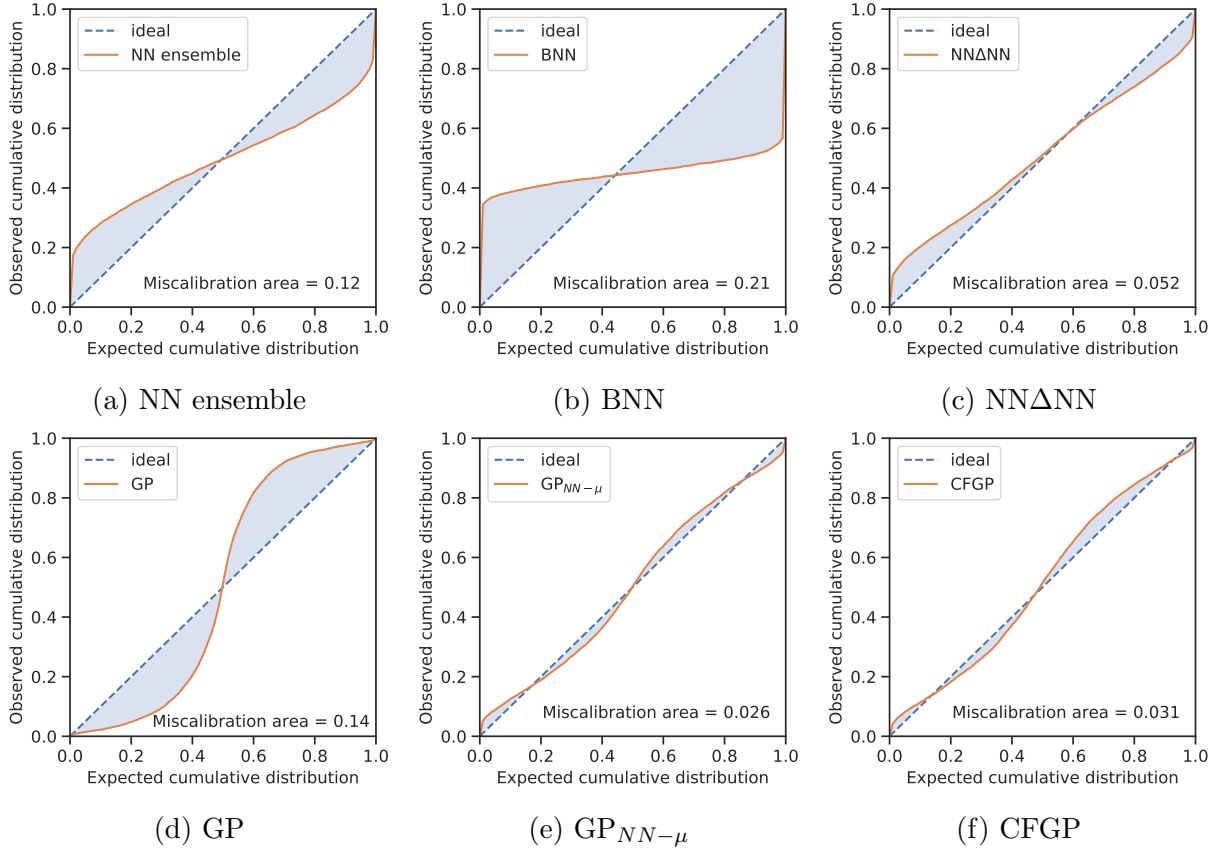
Figure 6: Calibration curves for all UQ methods used in this study. Dashed, blue lines indicate perfect calibration while solid orange lines indicate the experimental calibration of the test set. The blue, shaded area between these lines is defined as the miscalibration area.

Table 1: Performance metrics for all methods used in this study, which include: Median Absolute Error (MDAE), Mean Absolute Error (MAE), Root Mean Squared Error (RMSE), Mean Absolute Relative Percent Difference (MARPD), R^2 correlation coefficient (R^2), miscalibration area (MisCal), calibration error (CalErr), sharpness (Sha), and negative log-likelihood (NLL). The units of MDAE, MAE, RMSE, and sharpness are all in eV. The units of MARPD are in %. The miscalibration area, calibration error, and NLL are unitless. NLL values were all divided by 1,000 to improve readability.

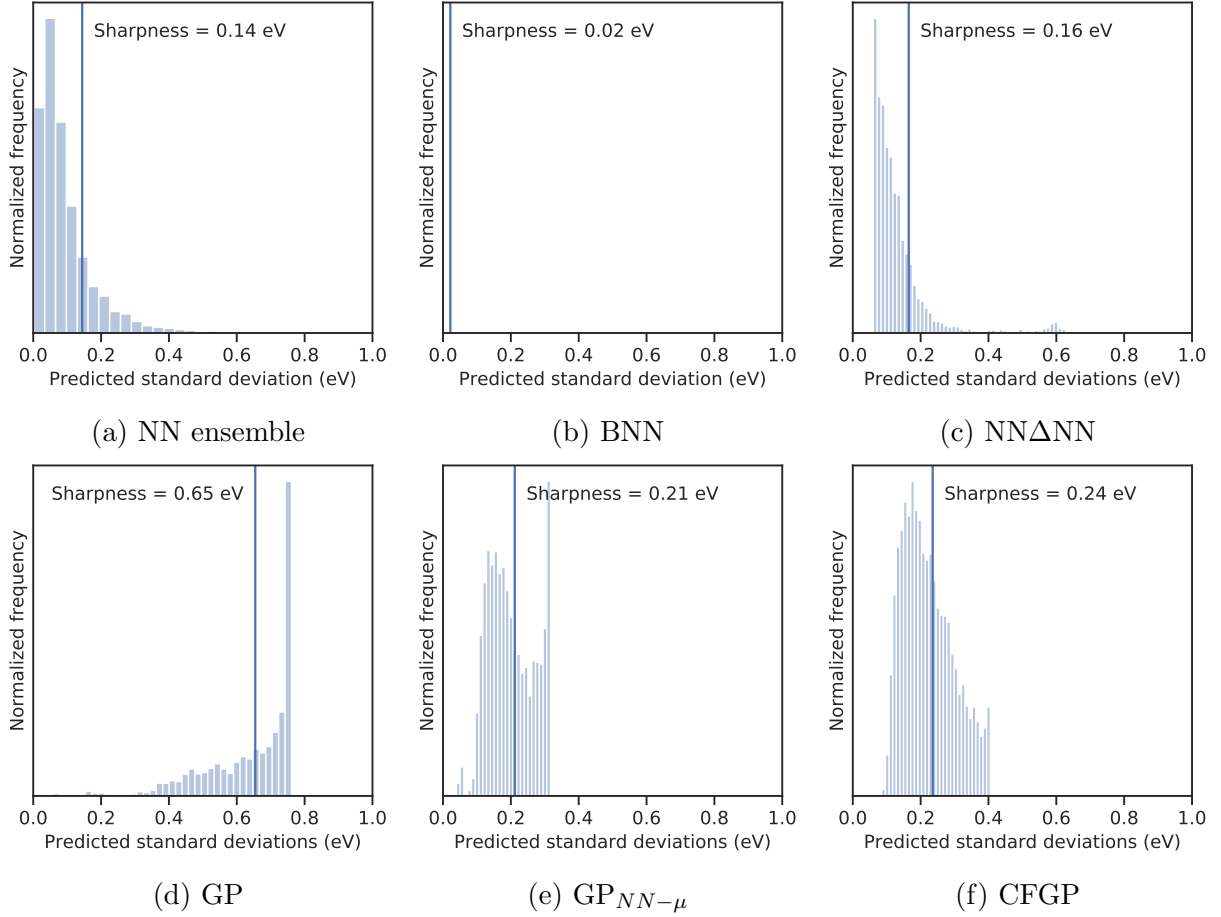| Method	MDAE	MAE	RMSE	MARPD	R^2	MisCal	CalErr	Sha	NLL
NN	0.11	0.19	0.34	61	0.80	N/A	N/A	N/A	N/A
NN ensemble	0.11	0.18	0.32	59	0.82	0.12	1.70	0.14	192.08
BNN	0.11	0.19	0.31	59	0.83	0.20	5.32	0.03	669.61
NNΔNN	0.11	0.19	0.34	59	0.80	0.05	0.39	0.16	18.61
GP	0.11	0.21	0.39	61	0.73	0.14	2.35	0.65	6.41
GP$_{NN-\mu}$	0.11	0.19	0.33	59	0.81	0.03	0.08	0.21	6.09
CFGP	0.11	0.19	0.33	59	0.80	0.03	0.13	0.24	2.80

Figure 7: Distribution plots of the ML-predicted standard deviations for each method. Sharpness values are indicated by vertical lines.

Regarding calibration: The NN ensemble and BNN are overconfident; the GP is under-confident; and the NNΔNN, GP$_{NN-\mu}$, and CFGP models are relatively calibrated. The three more calibrated methods all share a characteristic that the other methods do not: They all start with a NN that is dedicated for prediction alone, and then they end with some other in-series method to estimate uncertainty. Interestingly, this in-series method of learning predictions and then learning uncertainties is similar in spirit to how gradient boosted models "learn in stages" using an ensemble of models.

Regarding sharpness: The NN ensemble and BNN yield the sharpest uncertainties, although both do so at the cost of calibration. Among the three more calibrated models, the NNΔNN yields the lowest sharpness of 0.16 eV while the GP$_{NN-\mu}$ and CFGP yield sharpnesses of 0.21 and 0.24 eV, respectively. Note how GP-based UQ methods tend to yield less sharp uncertainties than methods based purely on NNs. This suggests that GPs may yield more conservative UQs.

Regarding NLL: The CFGP method yields the best (i.e., lowest) NLL value of *ca.* 2,800 while both the GP and GP$_{NN-\mu}$ models yield relatively moderate NLL values of *ca.* 6,000. Note how the under-confident GP model has a worse miscalibration area, calibration error, and sharpness than the NNΔNN but a better NLL value. Simultaneously, the two most over-confident and sharp models (NN ensemble and BNN) yield the worst NLL results. This shows that better NLL values correlate with relatively conservative estimates of UQ, but not with relatively liberal estimates. In other words: If we use NLL as our main performance metric, then we will favor under-confident UQ estimates in lieu of over-confident estimates.

Given the performance metrics for accuracy, calibration, sharpness, and NLL, we expect the CFGP or GP$_{NN-\mu}$ methods to yield the best performing UQ models for our dataset. When choosing UQ methods for different applications, other factors should be considered. For example: Although the GP$_{NN-\mu}$ method performed relatively well, it relied on hand-crafted features. If future researchers wish to use the GP$_{NN-\mu}$ method to predict other properties from atomic structures, they may have to define their own set of features. This

process of feature engineering is non-trivial and varies from application to application. In some cases, it may be easier to use a UQ method that does not require any additional features beyond the NN input, such as NNΔNN or CFGP. This is why declare CFGP as the method of choice for our study here; it has a relatively competitive accuracy, calibration, and sharpness while requiring less information than $GP_{NN-\mu}$.

Another factor to consider is the overhead cost of implementation. For example: The NN ensemble method is arguably the simplest NN-based UQ method used here and may be the easiest method to implement. Conversely, NN ensembles also have a higher computational training cost than some of the other methods used here, such as NNΔNN or CFGP. This high training cost is exacerbated if the ensemble is meant to be used in an active framework where the model needs to be trained continuously. As another example: The BNN method yielded perhaps the worst results of all the methods studied here. It could be argued that further optimization of the BNN could have resulted in higher performance. But creation and training of BNNs is still an active area of research with less literature and support than GPs or non-Bayesian NNs. This lack of support led to us spending nearly twice as long creating a BNN compared to the other methods. It follows that further optimization of the BNN would be non-trivial and may not be worth the overhead investment.

Conclusions

We examined a procedure for comparing different methods for uncertainty quantification (UQ). This procedure considers the accuracy of each method, the honesty of their uncertainty estimates (i.e., their calibration), and the size of their uncertainty estimates (i.e., their sharpness). To assess accuracy, we outlined a common set of error metrics such as MAE or RMSE, among others. To assess calibration, we showed how to create, interpret, and quantify calibration curves. To assess sharpness, we showed how to calculate and plot sharpness. To assess all three aspects simultaneously, we suggest using the negative log-likelihood (NLL)

as a performance metric. The ensemble of all these metrics and figures can be used to judge the relative performance of various UQ methods in a holistic fashion.

As a case study, we tested six different methods for predicting Density Functional Theory (DFT) calculated adsorption energies with UQ. The best performing method was a Convolution-Fed Gaussian Process (CFGP), which used a pre-trained convolutional output from a NN as features for a subsequent GP that made probabilistic predictions. Our studies also showed that the GP-based methods we tested tended to yield higher and more conservative uncertainty estimates than the methods that used only NNs and NN derivatives. We also found that in-series methods tended to yield more calibrated models—i.e., methods that use one model to make value predictions and then a subsequent model to make uncertainty estimates were more calibrated than models that attempted to make value and uncertainty predictions simultaneously. These results are limited to our dataset. Results may vary for studies with different applications, different models, or different hyperparameters. But the underpinning procedure we used to compare these models is still broadly applicable.

Note that it would be possible to recalibrate[16] each of the models in this study to improve their uncertainty estimates. We purposefully omitted recalibration in this study to (1) simplify the illustration of the UQ assessment procedure; (2) assess the innate performance of each of these UQ methods without confounding with recalibration methods; and (3) reduce overhead investment. Future work should consider recalibration if the feasible UQ methods provide insufficiently calibrated uncertainty predictions

Future work may also consider inductively biased UQs. For example: If we used the Bayesian Error Estimation Functional with van der Waals correlation (BEEF-vdW),[33] then our DFT calculated adsorption energies would have been distributions rather than single point estimates. Such distributions could be propagated to certain UQ surrogate models, e.g., as a variable-variance kernel in a GP-type method. As another example of inductively biased UQs: A model may be able to make low-uncertainty predictions on a DFT-optimized structure and then also make high-uncertainty predictions on a similar but

DFT-unoptimized structure. UQs do not need to be derived strictly from data. They may also be derived from previous knowledge.

Code availability

Visit `https://github.com/ulissigroup/uncertainty_benchmarking` for the code used to create the results discussed in this paper. The code dependencies are listed inside the repository.

Author information

Corresponding author email: zulissi@andrew.cmu.edu. The authors declare no competing financial interest.

Acknowledgments

References

(1) Medford, A. J.; Kunz, M. R.; Ewing, S. M.; Borders, T.; Fushimi, R. *ACS Catalysis* **2018**, *8*, 7403–7429.

(2) Gu, G. H.; Noh, J.; Kim, I.; Jung, Y. *Journal of Materials Chemistry A* **2019**, *7*, 17096–17117.

(3) Schleder, G. R.; Padilha, A. C. M.; Acosta, C. M.; Costa, M.; Fazzio, A. *Journal of Physics: Materials* **2019**, *2*, 1–46.

(4) Alberi, K. et al. *J. Phys. D: Appl. Phys* **2019**, *52*, 1–48.

(5) Settles, B. In *Synthesis Lectures on Artificial Intelligence and Machine Learning*; Brachman, R. J., Cohen, W. W., Dietterich, T. G., Eds.; Morgan & Claypool, 2012; p 100.

(6) Chu, W.; Zinkevich, M.; Li, L.; Thomas, A.; Tseng, B. *Proceedings of the ACM SIGKDD International Conference on Knowledge Discovery and Data Mining* **2011**, 195–203.

(7) Frazier, P. I. A Tutorial on Bayesian Optimization. 2018.

(8) Garnett, R.; Krishnamurthy, Y.; Xiong, X.; Schneider, J.; Mann, R. *Proceedings of the 29th International Conference on Machine Learning, ICML 2012* **2012**, *2*, 1239–1246.

(9) Kandasamy, K.; Neiswanger, W.; Zhang, R.; Krishnamurthy, A.; Schneider, J.; Poczos, B. Myopic Bayesian Design of Experiments via Posterior Sampling and Probabilistic Programming. 2018.

(10) Peterson, A. A. *Journal of Chemical Physics* **2016**, *145*.

(11) Torres, J. A. G.; Jennings, P. C.; Hansen, M. H.; Boes, J. R.; Bligaard, T. **2018**, *156001*, 1–6.

(12) Jinnouchi, R.; Lahnsteiner, J.; Karsai, F.; Kresse, G.; Bokdam, M. *Physical Review Letters* **2019**, *122*, 225701.

(13) Peterson, A. A.; Christensen, R.; Khorshidi, A. *Phys. Chem. Chem. Phys. Phys. Chem. Chem. Phys* **2017**, *19*, 10978–10985.

(14) Musil, F.; Willatt, M. J.; Langovoy, M. A.; Ceriotti, M. *Journal of Chemical Theory and Computation* **2019**, *15*, 906–915.

(15) Janet, J. P.; Duan, C.; Yang, T.; Nandy, A.; Kulik, H. J. *Chemical Science* **2019**, *10*, 7913–7922.

(16) Kuleshov, V.; Fenner, N.; Ermon, S. Accurate Uncertainties for Deep Learning Using Calibrated Regression. 35th International Conference on Machine Learning. Stockholm, Sweden, 2018.

(17) Tran, K.; Ulissi, Z. W. *Nature Catalysis* **2018**, *1*, 696–703.

(18) Tran, K.; Aini, P.; Back, S.; Ulissi, Z. W. *Journal of Chemical Information and Modeling* **2018**, *58*, 2392–2400.

(19) Kresse, G.; Hafner, J. *Physical Review B* **1993**, *47*, 558–561.

(20) Kresse, G.; Hafner, J. *Physical Review B* **1994**, *49*, 14251–14269.

(21) Kresse, G.; Furthmüller, J. *Computational Materials Science* **1996**, *6*, 15–50.

(22) Kresse, G.; Furthmüller, J. *Physical Review B* **1996**, *54*, 11169–11186.

(23) Hjorth Larsen, A. et al. *Journal of Physics: Condensed Matter* **2017**, *29*, 273002.

(24) Hammer, B.; Hansen, L. B.; Nørskov, J. *Physical Review B* **1999**, *59*, 7413–7421.

(25) Thompson, S. K. In *Sampling*, 3rd ed.; Shewhart, W. A., Wilks, S. S., Eds.; John Wiley and Sons Inc., 2012; Chapter 11, pp 139–156.

(26) Xie, T.; Grossman, J. C. *Physical Review Letters* **2018**, *120*, 145301.

(27) Back, S.; Yoon, J.; Tian, N.; Zhong, W.; Tran, K.; Ulissi, Z. W. *The Journal of Physical Chemistry Letters* **2019**, *10*, 4401–4408.

(28) Bingham, E.; Chen, J. P.; Jankowiak, M.; Obermeyer, F.; Pradhan, N.; Karaletsos, T.; Singh, R.; Szerlip, P.; Horsfall, P.; Goodman, N. D. **2018**, 0–5.

(29) Gardner, J. R.; Pleiss, G.; Bindel, D.; Weinberger, K. Q.; Wilson, A. G. GPyTorch: Blackbox Matrix-Matrix Gaussian Process Inference with GPU Acceleration. 32nd Conference on Neural Information Processing Systems (NeurIPS). 2018.

(30) Gneiting, T.; Raftery, A. E. *Journal of the American Statistical Association* **2007**, *102*, 359–378.

(31) Dawid, A. P.; Musio, M. *Metron* **2014**, *72*, 169–183.

(32) Lakshminarayanan, B.; Pritzel, A.; Blundell, C. Simple and Scalable Predictive Uncertainty Estimation using Deep Ensembles. 31st Conference on Neural Information Processing Systems (NIPS). 2017.

(33) Wellendorff, J.; Lundgaard, K. T.; Møgelhøj, A.; Petzold, V.; Landis, D. D.; Nørskov, J. K.; Bligaard, T.; Jacobsen, K. W. *Physical Review B - Condensed Matter and Materials Physics* **2012**, *85*, 32–34.